Ionization balance in semiconductor quantum-dot lasers

Janet L. Pan*
Research Laboratory of Electronics, Massachusetts Institute of Technology, Cambridge, Massachusetts 02139
(Received 2 July 1993)

The commonly assumed quasiequilibrium particle distribution with the same quasi-Fermi-level for all quantum-dot carriers in the same energy (conduction or valence) band is found *not* to be valid for a wide range of temperatures at the inversion populations and bound energy separations (greater than a LO phonon energy) used in the literature. Bound state occupation factors obtained from the steady state solution of rate equations describing the ionization balance in room-temperature 100-Å-radius GaAs quantum dots whose centers are separated by 400 Å are found to be very different from the quasiequilibrium distribution used in an example from the literature. In such quantum dots, bound state transitions result from collisions between charged particles via the Coulomb interaction, and from interband and intraband radiative processes. The critical free electron concentration above which collisional processes can establish a quasiequilibrium in the conduction band is found to exceed 10^{19} cm^{-3}. Our numerical solution is in good agreement with Pitaevskii's model from atomic physics of an electron random walk in energy as modeled by a Fokker-Planck equation. In our simple model, electrons are captured into a bound conduction band state via three-body recombination and phonon emission, and drop into lower energy bound states via a series of collisional deexcitations before combining with a valence band hole. Solution of the rate equations is standard in numerical studies of stimulated emission in atomic plasmas, but our present discussion is, to our knowledge, the first in the literature on semiconductor quantum-dot lasers.

I. INTRODUCTION

The optical transitions between discrete bound energies in ideal semiconductor quantum dots could be spectrally[1-4] very narrow. This has lead to speculation[1-4] that quantum-dot lasers could have efficiencies which are higher than those of conventional semiconductor lasers. Further, the possibility of having typical adjacent bound energy separations in quantum dots greater than k_BT could render the laser characteristics in quantum dots less[2,4] temperature sensitive than in conventional semiconductor lasers.

Having typical adjacent bound energy separations greater than k_BT could also render[5] inconsequential the intraband relaxation of bound quantum-dot carriers via phonon emission, since typical LO phonon energies in semiconductors have values on the order of the room temperature k_BT. When the intraband relaxation of bound quantum-dot carriers via phonon emission is unimportant, the scattering of bound carriers resulting from other processes must be considered, as discussed in Sec. II. These processes include collisions between a charge bound particle and a charged free particle, and could result[6] in a bound state transition or in ionization of the bound particle. Interband[7,8] and intraband[6] radiative processes are also summarized in Sec. II. We also discuss processes which affect the ionization state of a quantum dot: collisional ionization, photoionization, ionization through absorption of an LO phonon, as well as their inverse processes. We give numerical values for the rates of these processes.

In previous work,[6,9] we found that when the interaction of bound carriers with phonons is unimportant, intraband collisional and radiative processes affecting bound states occur on a time scale much longer than an interband spontaneous emission lifetime for the electron and hole concentrations assumed[1-4] in the literature. This result of our previous paper[9] casts serious doubts on the validity of assuming a quasiequilibrium in either energy (conduction or valence) band in quantum dots, as is commonly done in the literature. The assumption of quasiequilibrium is indicated by the same quasi-Fermi level (E_{Fc} or E_{Fv}) in the direction function[10]

$$f_{c,v}(E)=\frac{1}{1+\exp([E-E_{Fc,Fv}]/k_BT)}\ , \tag{1}$$

for all the carriers in the same energy band in all the quantum dots and barrier. The assumption of (1) within an energy band is justifiable[10-12] in *bulk* semiconductors where intraband (mainly carrier-phonon and carrier-carrier) scattering is much faster than the interband (conduction-to-valence band) radiative emission. Section III describes a condition under which local thermodynamic equilibrium (LTE) in either the conduction or valence band may be assumed in quantum dots.

The numerical solution presented in this paper of the rate equations governing the conduction band population distribution in a realistic quantum-dot structure confirms the inadequacy of (1). Figure 4 and Eq. (27) show this result to be valid for a wide range of temperatures. Solution of the rate equations is standard in numerical studies of stimulated emission in atomic plasmas, but this paper discusses semiconductor quantum-dot lasers.

Section IV gives details of our study state solution to the population rate equations for 100-Å-radius GaAs quantum dots whose centers are separated by 400 Å, a

particular example[4] already dealt with in the literature. We will find that at room temperature and at typical inversion populations assumed in the literature, most of the conduction band electrons remain free and do not remain in quantum-dot bound states. A careful study of our numerical results in this section yields a simple physical picture in which electrons captured into a quantum-dot bound conduction band state through three-body recombination and phonon emission drop into lower energy bound states through a series of collisional deexcitations before combining with a valence band hole. Our numerical solution is in good agreement with Pitaevskii's model from atomic physics of an electron random walk in energy as modeled by a Fokker-Planck equation.

In order to assess the validity of assuming (1), we will be comparing our results with work done at Caltech,[4] for 100-Å-radius GaAs quantum dots whose centers are separated by 400 Å. We will find that the numerical solution of the population rate equations for all the states in an energy band in all the quantum dots and barrier is inconsistent with the assumption of quasiequilibrium (1) used in this work.[4] We will use the materials parameters presented in previous[8] work for GaAs quantum dots surrounded by $Al_{0.3}Ga_{0.7}As$ barriers. GaAs has[13] a room-temperature bulk band gap of 1.424 eV, a spin-orbit splitting of 340 meV, a LO phonon energy of 35.34 meV, an index of refraction of 3.3, light hole, heavy hole, and conduction band effective masses at the Γ point of $0.082m_0$, $0.45m_0$, and $0.067m_0$, respectively, and a low frequency dielectric of $12.85\epsilon_0$. Bulk $Al_{0.3}Ga_{0.7}As$ has light hole, heavy hole, and conduction band effective masses at the Γ point of $0.096m_0$, $0.51m_0$, and $0.092m_0$, respectively, a conduction band edge which lies 289.1 meV above that in GaAs, a valence band edge which lies 192.7 meV below that in GaAs, and a room-temperature[14] low frequency dielectric of $12.01\epsilon_0$. Unless otherwise specified, we will assume room-temperature operation of our quantum-dot lasers throughout this paper.

II. PROCESSES AFFECTING QUANTUM-DOT BOUND CARRIERS

When intraband scattering is much slower than interband radiative emission in quantum dots, we cannot blithely assume that each energy (conduction or valence) band is described by the quasiequilibrium (1), as can be done in the bulk. This section considers the processes determining the steady state population of bound carriers in such quantum dots. The collisional excitation and ionization processes discussed in Secs. II A and II B are summarized from the literature.[6,15,16] Intraband and interband radiative bound-bound and bound-free transitions are summarized in Secs. II C and II D. The effects of LO phonons on the quantum-dot ionization balance and of acoustic phonons in equilibrating nearly degenerate bound states are discussed in Sec. II E.

We will assume that the *free* carriers, which have energies beyond the barrier band edge, are in a Fermi-Dirac quasiequilibrium (1) with other free carriers in the same energy band. For simplicity, we will assume that an equilibrium distribution describes the photons and phonons, although this condition can easily be modified.

A. Collisional excitation

Collisional excitation and deexcitation by incident electrons can be indicated by the forward and reverse reactions, respectively ($E_{ji}>0$),

$$X(Z,i)+e \rightleftharpoons X(Z,j)+e \ . \tag{2}$$

A similar equation can be written for incident holes. Here $X(Z,i)$ denotes the quantum dot which has a total charge of Z on it and an electron (hole) in state i. In collisional excitation processes, the incident free particle loses energy E_{ji} as it excites a bound particle in the quantum dot from state i to state j, via the Coulomb interaction between the two charged particles. The collisional deexcitation rate coefficient q_{ji}^f is related to the collisional excitation rate coefficient q_{ij}^f through the principle[17] of detailed balance:

$$q_{ji}^f=\frac{g_i}{g_j}q_{ij}^f \exp\left[\frac{E_{ji}}{k_B T}\right] , \tag{3}$$

where $f=c,v$ denotes the energy band (conduction or valence) containing the incident free particle and g_i is the degeneracy of the state i.

Appendix A summarizes our calculation of the colllisional excitation rate coefficients in quantum dots. A more detailed discussion of collisional excitation in quantum dots has been given previously.[6]

B. Collisional ionization

Collisional ionization and its inverse, three-body recombination, can be indicated by the forward and reverse reactions, respectively,

$$X(Z-1,i)+e \rightleftharpoons X(Z)+e+e \ , \tag{4}$$

for an incident electron and for i in the conduction band. A similar equation can be written for incident holes and/or for i in the valence band. In collisional ionization processes, the incident particle loses an energy of at least the ionization potential of the bound particle as it excites, via the Coulomb interaction between the two charged particles, the bound particle in the quantum dot from the bound state i to the continuum.

If we define $N(Z-1,i)$ as the concentration of quantum dots $X(Z-1,i)$ and $N(Z)$ as the concentration of the parent "ion" $X(Z)$, then the collisional ionization rate out of and the three-body recombination rate into state i are, respectively, $N(Z-1,i)n_f q_i^{fb}$ and $N(Z)n_f n_b \alpha_3^{fb}(i)$, where $f=c,v$ denotes the energy band (conduction or valence) containing the incident free particle, $b=c,v$ denotes the energy band containing the bound state i, and n_f, n_b denote free carrier concentrations. The principle[17] of detailed balance relates the coefficient for collisional ionization q_i^{fb} to that for three-body recombination $\alpha_3^{fb}(i)$,

$$\frac{q_i^{fb}}{\alpha_3^{fb}(i)} = \frac{g(Z)}{g(Z-1,i)} N_{b=C,V} \exp\left[\frac{-U(Z-1,i)}{k_B T}\right], \quad (5)$$

where the room temperature $N_C = 2(2\pi m_{\mathrm{DOS},C} k_B T/h^2)^{3/2}$ is 6.73×10^{17} cm^{-3} in $Al_{0.3}Ga_{0.7}As$ and 4.19×10^{17} cm^{-3} in GaAs, where $U(Z-1,i)$ is the ionization potential of the quantum dot with total charge $Z-1$ and a particle in state i, and where $g(Z)$ and $g(Z-1,i)$ are the statistical degeneracies of the initial and final quantum dot "ions."

Appendix B summarizes our calculation of the collisional ionization rate coefficients in quantum dots. A more detailed discussion of collisional ionization in quantum dots has been given previously.[6]

C. Intraband and interband bound-bound radiative processes

Radiative processes between bound states in a quantum dot can be either interband or intraband, as shown in Figs. 1 and 2. Interband radiative processes involve bound states in both the conduction and valence bands, such as states 1 and 1′ of Fig. 1. Intraband radiative processes involve bound states within the same energy band, such as states 2 and 3 of Fig. 2.

Spontaneous emission and photoexcitation can be indicated by the forward and reverse reactions, respectively ($E_{ji} > 0$)

$$X(Z,j) \rightleftharpoons X(Z,i) + h\nu \ . \quad (6)$$

Stimulated emission is indicated by

$$X(Z,j) + h\nu \rightarrow X(Z,i) + h\nu + h\nu \ . \quad (7)$$

Detailed balance relates the spontaneous[12] emission rate A_{ji} to the stimulated emission B_{ji} and photoexcitation B_{ij} (Einstein) coefficients:

$$\frac{n_r e^2 E_{ji}^2 \sum_{i,j} f_{ji}}{2\pi\hbar^2 c^3 m_0 \epsilon_0 g_j} = A_{ji} = \frac{8\pi n_r^3 h \nu_{ji}^3}{c^3} B_{ji} = \frac{8\pi n_r^3 h \nu_{ji}^3}{c^3} B_{ij} \frac{g_i}{g_j} \ , \quad (8)$$

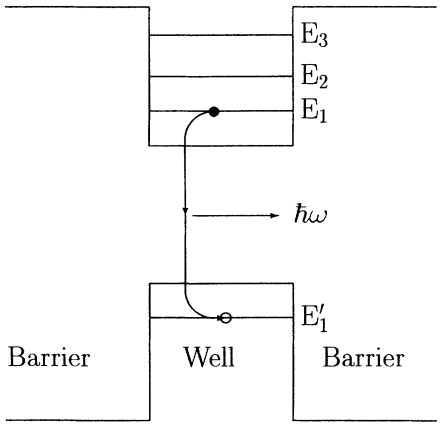

FIG. 1. Interband radiative processes involve bound states in both the conduction and valence bands, such as states 1 and 1′ in the figure.

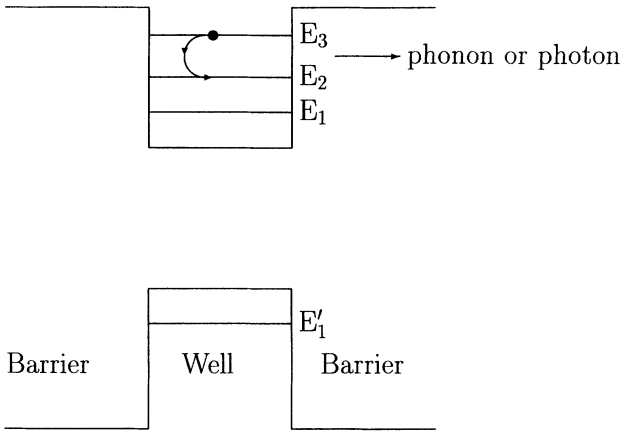

FIG. 2. Intraband transitions involve bound states within the same energy band, such as states 2 and 3 in the figure, and can be accomplished with the emission or absorption of either a photon or a phonon.

where the sum is over all degenerate initial (j) and degenerate final (i) states, n_r is the refractive index, g_j is the initial (upper) state degeneracy, $E_{ji} = h\nu_{ji}$, and f_{ji} is the oscillator strength.

The quantum-dot bound states used to calculate optical dipoles for both interband (conduction to valence band) and intraband transitions have been discussed in detail elsewhere.[6,7,18] These bound states are calculated in $\mathbf{k}\cdot\mathbf{p}$ theory.[19] In materials such as GaAs, where the energy band structure near $\mathbf{k}=0$ has an approximate spherical symmetry in wave vector space, it is possible to write all wave functions[7,18] as eigenstates of the total angular momentum, where the total single particle angular momentum is the vector sum of the electron spin, the microscopic or Bloch angular momentum which is associated with the cell-periodic part of the wave function, and the envelope angular momentum which is associated with the part of the wave function changing slowly over many unit cells. The effect of the rotationally symmetric potential formed by the barrier material surrounding the quantum dots is then included in a Schrödinger equation acting[7,18,19] on the envelope part of the wave function. Boundary conditions are satisfied by choosing the particle wave functions to be total angular momentum eigenstates.

The oscillator strengths for interband transitions have been calculated[7,8] in the literature. In Table III, $A_{cv}(i)$ is the average net spontaneous emission rate out of the bound conduction band state i; it denotes the average (over all valence band ionization configurations) of the sum of the spontaneous emission rates out of the bound conduction band state i to all bound valence band states occupied by a hole. [See Eq. (44) below.] The $A_{cv}(i)$ are seen to be the largest rates in Table III.

Intraband transitions differ from interband transitions in that the former involve a change in the symmetry of the carrier envelope function. In a previous paper, the bound-bound intraconduction band dipole (summed over degenerate initial and final bound states) was found to be

$$\sum_{F_{iz},F'_{iz}} |\langle \Phi_i|\mathbf{r}|\Phi'_{i'}\rangle|^2 = \begin{cases} R^2 \dfrac{(K_iR)^2(K'_iR)^2}{|(K_iR)^2-(K'_iR)^2|^4} \left[\dfrac{4(2F_i+1)}{3(F_i+1)}\dfrac{1}{F_i}\right] & \text{for } F'_i=F_i \\ R^2 \dfrac{(K_iR)^2(K'_iR)^2}{|(K_iR)^2-(K'_iR)^2|^4} \left[\dfrac{4(2F_i+1)}{3(F_i+1)}(2F_i+3)\right] & \text{for } F'_i=F_i+1 \ , \end{cases} \tag{9}$$

assuming that the conduction band wave functions have no valence band character, and where F is the total (spin plus Bloch plus envelope) angular momentum quantum number.

Table I shows the oscillator strengths for intraconduction band bound state transitions. These numerical values were obtained assuming[8,20] that the conduction band has a nonparabolic dispersion relation and that the conduction band wave functions have a small degree of valence band character appropriate to $\mathbf{k}\cdot\mathbf{p}$ theory. The oscillator strengths in Table I are in good agreement with the approximate values obtained from (9).

Tables II and III show that in our numerical example of 100-Å-radius GaAs quantum dots, the typical interband spontaneous emission is much faster than the typical intraband spontaneous emission. In Appendixes C and D, we show that when the bulk energy band gap is larger than the typical adjacent bound energy separations, the interband spontaneous emission will be faster than the intraband radiative emission. The consequence is that in order for LTE to be established in all of an energy band within the interband spontaneous emission lifetime, there must be an intraband process which acts on the bound carriers at a rate which is faster than both interband and intraband spontaneous emission, as we discuss in Sec. III.

TABLE I. Oscillator strengths (summed over the initial and final state degeneracies) for intra-conduction-band bound state transitions. The conduction band (Refs. 8 and 20) was modeled to have a nonparabolic dispersion relation and conduction band wave functions, whose symmetries are given in Table III, to have a small degree of valence band character as appropriate to $\mathbf{k}\cdot\mathbf{p}$ theory. The oscillator strengths in this table are in good agreement with the approximate values obtained from (9).

Initial level i	Final level j	$\sum_{F_{iz},F'_{iz}} f_{i'i}$	Initial level i	Final level j	$\sum_{F_{iz},F'_{iz}} f_{i'i}$
0	1	8.58	2	7	5.60
0	2	16.86	2	8	1.41
0	4	1.34	2	9	7.81×10^{-4}
0	5	7.39×10^{-4}	3	6	90.01
0	8	0.222	3	7	4.60
0	9	0.433	3	9	14.59
1	4	27.05	4	5	0.0173
1	5	4.20	4	7	63.54
1	8	1.95×10^{-3}	4	8	7.99
1	9	1.41	4	9	1.73
2	3	48.29	5	8	10.68
2	4	5.47	5	9	20.39
2	5	8.02	7	9	0.111

D. Bound-free radiative processes

Spontaneous radiative recombination of free electrons into a bound state i and photoionization of electrons from a bound state i into the continuum can be indicated by the forward and reverse reactions, respectively,

$$X(Z)+e \rightleftharpoons X(Z-1,i)+h\nu \ . \tag{10}$$

Stimulated radiative recombination is indicated by

$$X(Z)+e+h\nu \rightarrow X(Z-1,i)+h\nu+h\nu \ . \tag{11}$$

Similar equations for holes can be written when i is a valence band state. An example of the spontaneous radiative recombination of a free electron into a bound state is shown in Fig. 3.

The photoionization, stimulated radiative recombination, and spontaneous radiative recombination rates from/into the bound state i are $N(Z-1,i)\beta_{pi}(i)$, $N(Z)n_{c,v}\beta_{rr}(i)$, and $N(Z)n_{c,v}\alpha(i)$. The coefficients for photoionization $\beta_{pi}(i)$, stimulated radiative recombination $\beta_{rr}(i)$, and spontaneous radiative recombination $\alpha(i)$ are

$$\beta_{pi}(i)=\frac{1}{g_i}\int_0^\infty A_{ji}(E_j+U_i)n(\hbar\omega)L^3g(E_j)dE_j \tag{12}$$

and

$$n_b[\beta_{rr}(i)+\alpha(i)] = \int_0^\infty A_{ji}(E_j+U_i)[n(\hbar\omega)+1]f(E_j)L^3g(E_j)dE_j \ , \tag{13}$$

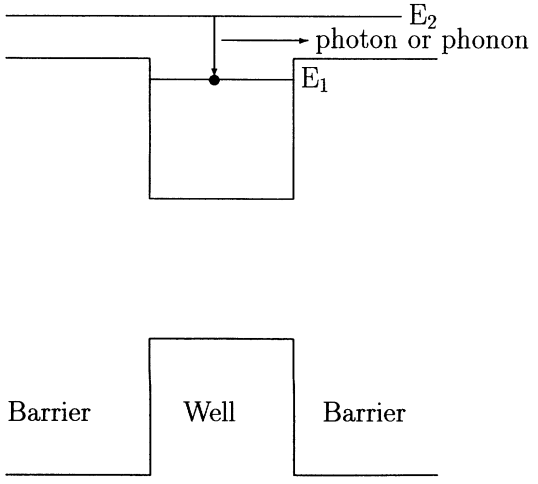

FIG. 3. Capture of a free electron into the bound state 1 can be accomplished by the spontaneous or stimulated emission of a photon or a phonon.

TABLE II. Room-temperature intraband collisional (de)excitation and radiative rates affecting the ten conduction band single particle bound states in a 100-Å radius GaAs quantum dot. Intraband collisional rates are usually largest and intraband radiative rates are smallest for those states which have the smallest energy difference. The free electron concentration was taken to be $n_c = 1.493 \times 10^{16}$ cm^{-3} from the solution of the rate equations (29).

Initial level i	Final level j	Collisional rate $n_c q_{ij}^c$ (1/s)	Radiative rate $A_{ij}(n+1)$ or $B_{ij}n$ (1/s)	Initial level i	Final level j	Collisional rate $n_c q_{ij}^c$ (1/s)	Radiative rate $A_{ij}(n+1)$ or $B_{ij}n$ (1/s)
0	1	5.70×10^{6}	2.57×10^{5}	4	7	4.70×10^{6}	8.18×10^{5}
0	2	1.12×10^{7}	5.05×10^{5}	4	8	1.48×10^{4}	4.72×10^{4}
0	4	4.68×10^{3}	1.56×10^{4}	4	9	3.23×10^{3}	1.02×10^{4}
0	5	3.19×10^{-1}	4.47×10^{0}	5	0	7.61×10^{1}	1.06×10^{3}
0	8	3.26×10^{-1}	1.29×10^{2}	5	1	3.18×10^{6}	2.48×10^{6}
0	9	6.35×10^{-1}	2.52×10^{2}	5	2	6.07×10^{6}	4.75×10^{6}
1	0	4.29×10^{7}	1.93×10^{6}	5	4	4.88×10^{5}	1.47×10^{3}
1	4	7.46×10^{6}	7.52×10^{5}	5	8	3.75×10^{5}	2.16×10^{5}
1	5	1.00×10^{5}	7.85×10^{4}	5	9	7.17×10^{5}	4.12×10^{5}
1	8	8.67×10^{-2}	5.07×10^{0}	6	3	4.65×10^{7}	8.09×10^{6}
1	9	6.29×10^{1}	3.68×10^{3}	7	2	2.91×10^{5}	2.26×10^{6}
2	0	4.21×10^{7}	1.90×10^{6}	7	3	3.17×10^{6}	5.52×10^{5}
2	3	6.66×10^{6}	6.71×10^{5}	7	4	4.38×10^{7}	7.62×10^{6}
2	4	7.56×10^{5}	7.62×10^{4}	7	9	5.38×10^{4}	1.15×10^{3}
2	5	9.59×10^{4}	7.49×10^{4}	8	0	2.06×10^{3}	8.18×10^{5}
2	7	2.91×10^{3}	2.26×10^{4}	8	1	7.27×10^{1}	4.26×10^{3}
2	8	3.15×10^{1}	1.84×10^{3}	8	2	5.28×10^{4}	3.09×10^{6}
2	9	1.73×10^{-2}	1.01×10^{0}	8	4	2.32×10^{6}	7.39×10^{6}
3	2	4.77×10^{7}	4.80×10^{6}	8	5	9.94×10^{6}	5.72×10^{6}
3	6	4.44×10^{6}	7.72×10^{5}	9	0	2.01×10^{3}	7.97×10^{5}
3	7	2.27×10^{5}	3.95×10^{4}	9	1	2.64×10^{4}	1.54×10^{6}
3	9	1.81×10^{4}	5.75×10^{4}	9	2	1.45×10^{1}	8.52×10^{2}
4	0	1.89×10^{5}	6.32×10^{5}	9	3	2.12×10^{6}	6.75×10^{6}
4	1	4.01×10^{7}	4.03×10^{6}	9	4	2.52×10^{5}	8.03×10^{5}
4	2	8.12×10^{6}	8.18×10^{5}	9	5	9.49×10^{6}	5.45×10^{6}
4	5	8.27×10^{4}	2.50×10^{2}	9	7	4.51×10^{5}	9.67×10^{3}

respectively, where E_j is the free particle energy measured from the barrier band edge; $E_j + U_i$ is the energy of the bound-free radiative transition; $A_{ji}(E_j + U_i)$ is the Einstein A coefficient (8), which is written with its explicit dependence on the free particle energy, of the bound-free radiative transition; $f(E)$ is the free particle (Fermi-Dirac) energy distribution; $L^3 g(E)$ is the free particle density of states per unit energy; the explicit L^3 in the formulas will be canceled by the free particle normalization; and

$$n(\hbar\omega = E_j + U_i) = \frac{1}{\exp(\hbar\omega/k_B T) - 1} \ . \tag{14}$$

The photoionization and radiative recombination coefficients manifestly satisfy the principle of detailed balance

$$\alpha(i) + \beta_{rr}(i) = \frac{\beta_{pi}(i)}{N_b} \frac{g(Z-1,i)}{g(Z)} \exp\left[\frac{U_i}{k_B T}\right] , \tag{15}$$

where $b = C$ or V.

The use of a Planck distribution in (14) is valid, except at the frequencies of any stimulated emission, for a semiconductor in thermal contact with equilibrium surroundings. The reason is that typical semiconductors have macroscopic dimensions and are thus much larger than the optical depth (inverse absorption coefficient) at the frequencies of interest. A thermal distribution of photons is consistent with a population inversion in semiconductor lasers, since it is the injection current and not the photon distribution which determines the population distribution in each energy band.

The integrals (12) and (13) were computed numerically and checked with the analytical results of previous work.[6]

E. Carrier-phonon interaction

LO phonons could enable the recombination into (see Fig. 3) and ionization out of those bound energies which are within a LO phonon energy of the barrier band edge, as indicated by the reactions

$$X(Z) + e \rightleftharpoons X(Z-1,i) + \hbar\omega_{\mathrm{LO}} \tag{16}$$

and

TABLE III. Room-temperature collisional ionization, three-body recombination, photoionization, radiative recombination, and total interband spontaneous emission rates for ten conduction band single particle bound states in a 100-Å radius GaAs quantum dot. As discussed in the text, three-body recombination is the dominant capture process into weakly bound single particle states which are located more than an LO phonon energy below the barrier band edge. $A_{cv}(i)$ is the average (over all valence band ionization configurations) net spontaneous emission rate out of the conduction band bound state i. Interband radiative emission is the dominant process depopulating lower energy conduction band bound states. Radiative recombination is insignificant, mainly as a result of the relatively small ionization potentials for the quantum-dot bound states. Not shown are the lifetimes associated with ionization through absorption of a LO phonon, which at typical values of 0.1 ps are much faster than all other rates. Electrons in the single particle bound states 8,9 are within a LO phonon energy of the barrier band edge at 289.1 meV and are in equilibrium with the free electrons. The free electron concentration was found from solution of the rate equations (29) to be $n_c=1.493\times10^{16}$ cm^{-3} out of a total of $n_{c,\mathrm{tot}}=3.125\times10^{16}$ cm^{-3} [two electrons and two holes in every (400 Å)^3] carriers in the conduction band. The bound state energy levels and symmetries have been discussed (Ref. 8) elsewhere. All energies are measured from the GaAs conduction band edge.

Level number i	Conduction band state	Energy (meV)	Collisional ionization rate $n_c q_i^{cc}$ (1/s)	Three-body recombination rate $n_c^2\alpha_{33}^{cc}(i)$ (1/s)	Photoionization rate $\beta_{pi}(i)$ (1/s)	Radiative recombination rate $n_c\alpha(i)$ (1/s)	Total interband spontaneous emission rate $A_{cv}(i)$ (1/s)
0	$1S_{1/2}$	53.7	5.46×10^{2}	2.05×10^{5}	5.46×10^{0}	2.05×10^{3}	1.58×10^{8}
1	$1P_{1/2}$	105.9	8.92×10^{3}	4.44×10^{5}	3.47×10^{1}	1.73×10^{3}	1.06×10^{8}
2	$1P_{3/2}$	105.9	8.92×10^{3}	8.88×10^{5}	3.79×10^{1}	3.77×10^{3}	7.86×10^{7}
3	$1D_{5/2}$	167.4	2.86×10^{5}	3.98×10^{6}	1.44×10^{3}	2.01×10^{4}	4.08×10^{7}
4	$1D_{3/2}$	167.4	2.86×10^{5}	2.66×10^{6}	1.39×10^{3}	1.29×10^{4}	6.22×10^{7}
5	$2S_{1/2}$	195.4	1.59×10^{6}	2.50×10^{6}	3.08×10^{3}	4.85×10^{3}	5.67×10^{7}
6	$1F_{7/2}$	235.6	2.63×10^{7}	3.49×10^{7}	8.38×10^{3}	1.11×10^{4}	2.13×10^{7}
7	$1F_{5/2}$	235.6	2.63×10^{7}	2.62×10^{7}	7.98×10^{3}	7.95×10^{3}	3.58×10^{7}
8	$2P_{1/2}$	280.2	5.08×10^{9}	3.02×10^{8}	1.03×10^{4}	6.11×10^{2}	3.02×10^{7}
9	$2P_{3/2}$	280.2	5.08×10^{9}	6.03×10^{8}	1.12×10^{4}	1.32×10^{3}	3.11×10^{7}

$$X(Z)+e+\hbar\omega_{\mathrm{LO}}\rightarrow X(Z-1,i)+\hbar\omega_{\mathrm{LO}}+\hbar\omega_{\mathrm{LO}}\ . \quad (17)$$

Based on our other numerical work,[21] we assumed that the phonon assisted ionization rate is

$$\beta_{\mathrm{LO},i}(i)=(0.1\ \mathrm{ps})^{-1}\ , \quad (18)$$

which is also very similar to bulk[11] LO phonon scattering rates.

For an equilibrium (Bose-Einstein) distribution of LO phonons, the LO phonon assisted recombination rate of free electrons into a bound state is related to the LO phonon assisted ionization rate by detailed balance

$$\alpha_{\mathrm{LO},r}(i)+\beta_{\mathrm{LO},r}(i)=\frac{\beta_{\mathrm{LO},i}(i)}{N_b}\frac{g(Z-1,i)}{g(Z)}\exp\left[\frac{U_i}{k_BT}\right]\ . \quad (19)$$

The use of a Planck distribution for phonons is justifiable in a lattice which is in thermal contact with equilibrium surroundings and which is in the absence of nonequilibrium phonon sources, such as an externally applied vibration of the lattice or temperature gradients.

The LO phonon modes in a quantum dot are quantized because the bulk LO phonon energies differ in the dot and barrier materials. In a previous work,[21] we have shown that the quantization of the LO phonons does not greatly affect any process in which all LO phonon modes participate, such as the example discussed in this paper of the LO phonon coupling of a weakly bound electron state to the continuum. The reason is that the quantization results in fewer LO phonon modes in the quantum dot than in the bulk, but the strength of the interaction of each mode is proportionately[21,22] greater. Thus, the use of either bulk or quantized LO phonon modes does not greatly affect the numerics of this paper.

Emission and absorption of an acoustic phonon, as indicated by the reactions

$$X(Z,j)+\hbar\omega_{\mathrm{ac}}\rightarrow X(Z,i)+\hbar\omega_{\mathrm{ac}}+\hbar\omega_{ac} \quad (20)$$

and

$$X(Z,j)\rightleftharpoons X(Z,i)+\hbar\omega_{\mathrm{ac}}\ , \quad (21)$$

result in bound state transitions, as shown schematically in the intraband transition of Fig. 2. Electronic bound state transitions resulting from interaction with phonons are ignored in much of the work on quantum dots because electronic bound state separations are greater than a LO phonon energy. In our numerical work, some bound states are degenerate or almost degenerate. In such cases, we will assume the acoustic[11,21] phonon assisted excitation rates $W_{\mathrm{ac},ij}$ are

$$W_{\mathrm{ac},ij}=(10.0\ \mathrm{ps})^{-1} \quad (22)$$

and that the acoustic phonon assisted deexcitation rates $W_{\mathrm{ac},ji}$ for an equilibrium distribution of acoustic phonons are found through detailed balance

$$W_{\mathrm{ac},ji} = \frac{g_i}{g_j} W_{\mathrm{ac},ij} \exp\left[\frac{E_{ji}}{k_B T}\right] . \quad (23)$$

(These energy degeneracies could be lifted by the Coulomb interaction between bound particles or by the nonideal fabrication of quantum dots. Carriers in states between which there is just a small energy separation will also be in LTE because of interaction with acoustic phonons.) The fast acoustic phonon scattering relative to interband spontaneous emission creates a LTE among degenerate or almost degenerate bound states.

The phonon scattering rates (18) and (22) are used in Sec. IV in calculating the quantum-dot ionization balance. The exact values of the LO and acoustic phonon scattering rates are not important. It is only significant that these rates are very large, much larger than that of interband spontaneous emission, and will create a LTE among those states connected by phonon processes.

III. CRITICAL FREE CARRIER CONCENTRATION FOR LTE IN AN ENERGY BAND

In the collisional-radiative recombination of free electrons with atomic ions, Pert[23] has stated that a requirement for LTE in an energy band is that collisional processes relax electrons into the lowest bound state in that energy band much more quickly than the spontaneous emission to all lower energy states. In our quantum-dot example, the energy band is the conduction[24] band the spontaneous emission is to all valence band states. Thus, the critical free carrier concentration $n_{c,\mathrm{crit}}$ for LTE to exist in the conduction band is

$$\left[\frac{E_{ji,\mathrm{typical}}}{U_j}\right] n_{c,\mathrm{crit}} q_{ji}^{c} \Big|_{E_{ji,\mathrm{typical}}} = 10 A_{cv}(j) . \quad (24)$$

The fraction $(U_j/E_{ji,\mathrm{typical}})[n_{c,\mathrm{crit}} q_{ji}^{c}|_{E_{ji,\mathrm{typical}}}]^{-1}$ is roughly the time it takes for an electron to lose an energy of U_j in increments of $E_{ji,\mathrm{typical}}$ via collisions. The *typical* conduction band bound state energy separation $E_{ji,\mathrm{typical}}$ is the appropriate energy separation to consider for a collisional cascade through the conduction band bound states. (The adjacent bound energy separation in quantum dots is fairly constant, unlike the situation in atomic ions where the adjacent bound energy separation is smaller for higher energy bound states. For our example, Table III shows adjacent quantum-dot bound states to be separated by about 40–60 meV.)

We are justified in assuming a collisional cascade in (24) because we shall see that at room temperature and the free carrier concentration of Sec. IV, bound electrons deexcite mainly by collisional rather than intraband radiative processes. Bound carriers deexcite via an intraband collisional cascade when the free carrier concentration satisfies

$$n_c q_{ji}^{c} > A_{ji} \quad (\text{for a typical } E_{ji}) , \quad (25)$$

where the energy E_{ji} is the typical adjacent bound state energy separation. [When (25) is satisfied, LTE does not exist within an energy band unless interband radiative processes are also slower than the collisional rates, as discussed in (24).] The critical free carrier concentration defined in (25) is usually very small, on the order of 10^{15} cm^{-3} for the "typical E_{ji}," of the $j=1$ (the $1P_{1/2}$ state) to $i=0$ (the $1S_{1/2}$ state) transition. Our free carrier concentration in Sec. IV of 1.493×10^{16} cm^{-3} satisfies (25).

The curve labeled "Pert" in Fig. 4 shows the temperature dependence of Pert's[23] critical free carrier concentration (24) for $i=1$ and $j=0$ in our 100-Å-radius GaAs quantum dots. The collisional rate coefficients used in Fig. 4 were obtained from the classical path model (49).

The free electron concentration $n_c = 1.493\times10^{16}$ cm^{-3} of Sec. IV is much smaller than the typical value of $n_{c,\mathrm{crit}}$ shown in Fig. 4 to be about 10^{19} cm^{-3}. [In a previous paper,[9] we showed that the erroneous assumption of (1) for *all* states in an energy band in all the quantum dots and barrier leads to a free carrier concentration of $n_c = 8.50\times10^{13}$ cm^{-3}, which is even further from satisfying (24).] Thus, by Pert's criterion (24), collisional excitation is not strong enough to establish a quasiequilibrium (1) among all the conduction band states.

Figure 5 shows that at free carrier concentrations greater than the critical value of (24), the quantum-dot conduction band bound state populations are described by a LTE. The figure shows the room-temperature concentrations of singly ionized quantum dots,

$$g(Z=1,i=9)N(Z=1,i)/g(Z=1,i)N(Z=1,i=9) ,$$

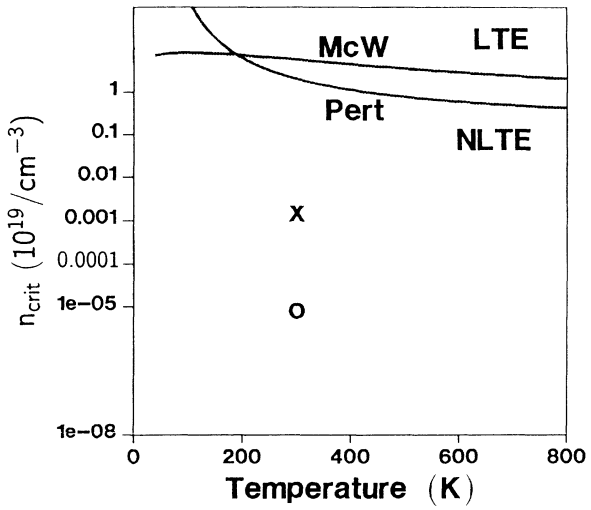

FIG. 4. The temperature dependence of the critical free carrier concentration defined by Pert and McWhirter in Sec. III. For Pert we use $i=1$ (the $1P_{1/2}$ state) and $j=0$. For McW we use the two most widely separated conduction band bound states $i=0$ [the $1S_{1/2}$ state of the literature (Ref. 20)] and $j=9$ (the $2P_{3/2}$ state). When the free electron concentration exceeds this $n_{c,\mathrm{crit}}$ all conduction band bound states are in quasiequilibrium. The point labeled × is the room-temperature free carrier concentration of 1.493×10^{16} cm^{-3} found from the numerical solution of the population rate equations in Sec. IV for 100-Å-radius GaAs quantum dots whose centers are separated by 400 Å. The point labeled ○ is the room-temperature free carrier concentration of 8.50×10^{13} cm^{-3} obtained (Ref. 9) by assuming (1) for all the carriers in the conduction band of the same quantum dots and barrier. In either case, (24) is not satisfied.

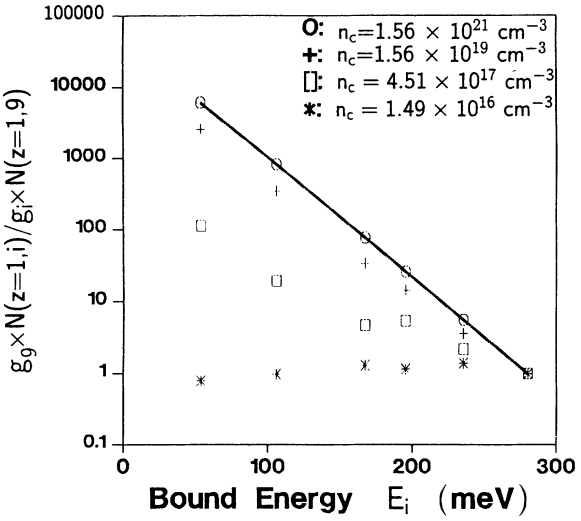

FIG. 5. The room-temperature concentrations of singly ionized quantum dots,

$$\frac{g(Z=1,i=9)N(Z=1,i)}{g(Z=1,i)N(Z=1,i=9)} ,$$

normalized to the concentration of singly ionized quantum dots having one electron in the highest energy bound state 9, as a function of the bound electron energy E_i for various values of the free electron concentration for our 100-Å-radius GaAs quantum dots whose centers are separated by 400 Å. The ion populations corresponding to the critical free carrier concentration in (24) of 1.56×10^{19} are indicated by crosses and are very close to the Saha-Boltzmann equilibrium (26) values, indicated by the solid line. The normalized ion populations corresponding to free carrier concentrations less than that in (24) are seen to be much smaller than the Saha-Boltzmann values.

normalized to the concentration of singly ionized quantum dots having one electron in the highest energy bound state 9, as a function of the bound electron energy E_i for various values of the free electron concentration for our 100-Å-radius GaAs quantum dots whose centers are separated by 400 Å. These ion concentrations are obtained from solution of the population rate equations, as described in Sec. IV. The solid line corresponds to the Saha-Boltzmann equilibrium[25]

$$N(Z=1,i)=N(Z+1)\frac{g(Z,i)}{g(Z+1)}\frac{n_c}{N_c}\exp\left[\frac{U_i}{k_BT}\right] , \quad (26)$$

where i is a bound conduction band state. The ion population corresponding to the critical free carrier concentration in (24) of 1.56×10^{19} are indicated by the crosses in Fig. 5 and are very close to the Saha-Boltzmann equilibrium values. The normalized ion populations corresponding to free carrier concentrations less than that in (24) are seen to be much smaller than the Saha-Boltzmann values.

To check our numerical evaluation of $n_{c,\mathrm{crit}}$ in Fig. 4, we now compare (24) with another criterion from the atomic physics literature for establishing LTE in an energy band. McWhirter's[15,26] criterion for quasiequilibrium (1) to exist within a band of bound energy states of ions in a plasma is that collisional deexcitation rates $n_{c,v}q_{ji}^{c,v}$ be much greater than the spontaneous radiative rates A_{ji} for all pairs i,j of bound states in the energy band. The critical free carrier concentration is defined as that concentration at which collisional deexcitation is ten times faster than the intraband spontaneous emission between the bound states i,j (in the same energy band) with the *largest* energy separation,

$$n_{c,\mathrm{crit}}q_{ji}^{c}=10A_{ji} . \quad (27)$$

The reasoning in (27) is that collisional excitation is the dominant process by which bound particles are excited upward when the energy difference E_{ji} is large. In order for the populations of states i and j to be in LTE, the dominant downward process must be the inverse (in the

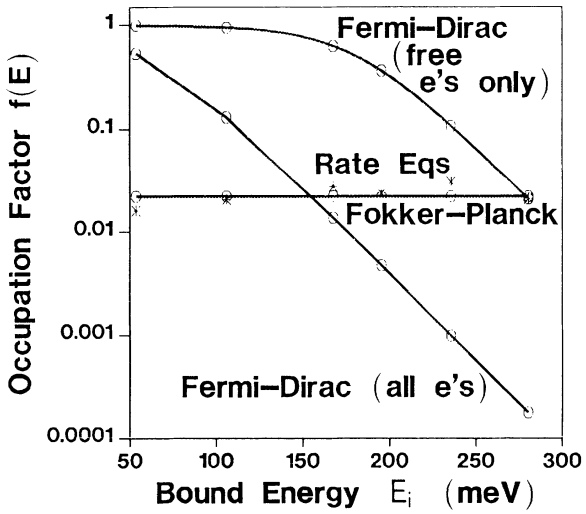

FIG. 6. The vast discrepancy at room temperature between occupation factors obtained from our Rate Eqs (labeled as stars) solution (34) and the quasiequilibrium distribution function (1) [Fermi-Dirac (all e's) with $E_{Fc}=56.7$ meV corresponding to two electrons per quantum dot] commonly assumed in the literature for *all* conduction band electrons. The Fermi-Dirac (all e's) distribution is assumed in work done at Caltech (Ref. 4). All numbers in this figure are for the conduction band of 100-Å-radius GaAs quantum dots whose centers are separated by 400 Å. Our rate equation solution is in good agreement with a simple model (Ref. 28) of the random walk, as described by a Fokker-Planck equation, of electrons in energy. A quasiequilibrium was assumed for all holes and for *free* electrons. Any electrons in quasiequilibrium with the *free* electrons would have the distribution labeled Fermi-Dirac (free e's only). For example, the electrons in the bound states at 280.2 meV, which is well within a LO phonon energy of the $Al_{0.3}Ga_{0.7}As$ band edge at 289.1 meV, are clearly seen to be in quasiequilibrium with the free electrons. The solid lines representing the Fermi-Dirac equilibrium for all and for free electrons only do not coincide because of differing values of the free electron concentration [where $N_c/N_C\simeq\exp(E_{Fc}/k_BT)$]: the assumption of a Fermi-Dirac distribution for *all* electrons yields a free electron concentration (Ref. 9) of 8.50×10^{13} cm^{-3}, while the Fermi-Dirac (free e's only) distribution in the figure assumed the free carrier concentration of 1.493×10^{16} cm^{-3} found in Sec. IV.

detailed balance sense) of collisional excitation, whence the requirement (27). A formula for $n_{c,\mathrm{crit}}$ in terms of the Van Regemorter collisional excitation rate coefficient is given[9] in the literature.

The curve labeled "McW" in Fig. 4 shows the temperature dependence of McWhirter's[15,26] critical free carrier concentration (27) for the two most widely separated conduction band bound states $i=0$ and $j=9$ in our 100-Å-radius GaAs quantum dots. Pert's $n_{c,\mathrm{crit}}$ is very similar to McWhirter's except at low temperatures. At low temperatures, Pert's $n_{c,\mathrm{crit}}$ is much larger than McWhirter's because (24) requires that both collisional *excitation* and deexcitation be much faster than interband radiative emission.

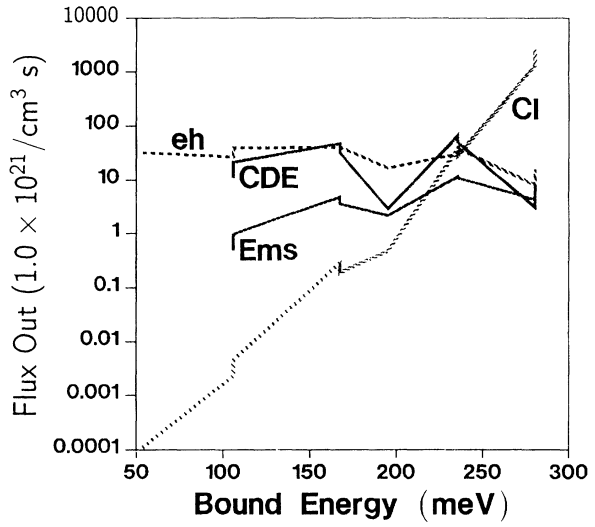

FIG. 7. Flux (concentration per unit time) at room temperature and a free electron concentration of $n_c = 1.493 \times 10^{16}$ cm^{-3} depopulating those quantum-dot ions having exactly one electron as a function of the energy of the one bound electron. Depopulation of these singly ionized quantum dots is accomplished mainly through interband radiative processes (*eh*) and intraband collisional deexcitation (CDE). This figure and Fig. 8 show that after an electron is captured from the extended continuum into a weakly bound state, it drops into lower energy bound states via collisional deexcitation until it combines with a valence band hole. For visual ease in this figure and in Fig. 8, straight lines have been drawn through the points associated with each discrete bound energy. Depopulation by intraband emission (Ems) and absorption (not shown) are weaker than intraband collisional processes at this free carrier concentration because the typical adjacent bound state energy separations are relatively small (the regime of collisional cascade of Sec. III). Collisional ionization (CI) is important mainly for bound states in the extended continuum, such as those at 280.2 meV. Not shown in this figure or in Fig. 8 are the fluxes, which are much larger than the fluxes shown in these figures and which affect only the states at 280.2 meV, associated with ionization (or recombination) through absorption (or emission) of a LO phonon. Observe that there are no bound states into which electrons originating in the lowest bound states at 53.7 meV can collisionally deexcite or emit (Ems) via an intraband transition. Contributions from quantum-dot ions having exactly two bound electrons were not considered in this figure or in Fig. 8.

In summary, we expect that the occupation of the bound states in the conduction band of our quantum dot cannot be described by a quasiequilibrium distribution, but that electrons will drop through the bound states by a collisional cascade. This is confirmed in Sec. IV. The actual occupation factors $f(E)$ given in Fig. 6 as the asterisks labeled "Rate Eqs" are very different from those in quasiequilibrium (1). Figures 7 and 8 indeed show that the downward cascade through the conduction band states is via collisional deexcitation and not intraband radiative processes.

IV. THE IONIZATION BALANCE

In this section, we solve the rate equations for the steady state ionization balance for a particular quantum-dot example taken from the literature. We determine which processes are most important and find a simple model for understanding the quantum-dot bound state population distribution.

The time rate of change of the concentration of quantum-dot ions is

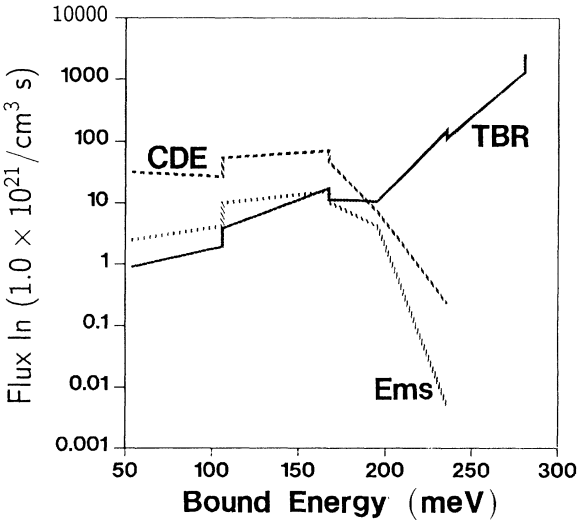

FIG. 8. Flux (concentration per unit time) at room temperature and a free electron concentration of $n_c = 1.493 \times 10^{16}$ cm^{-3} populating those quantum-dot ions having exactly one electron as a function of the energy of the one bound electron. At this free carrier concentration and relatively small typical adjacent bound state energy separations, population of the singly ionized quantum dots is mainly via collisional deexcitation (CDE) and not radiative (Ems) intraband transitions (the regime of collisional cascade of Sec. III). Three-body recombination (TBR) is important mainly for bound states in the extended continuum, such as those at 280.2 meV. Population of the bound states via radiative recombination is insignificant, as shown in Table III, mainly as a result of the relatively small ionization potentials for the quantum-dot bound states. Insignificant fluxes were found to result from processes which appeared in Tables II and III but which are not shown in Figs. 8 and 7. Observe that there are no bound states from which intraband collisional deexcitation or emission could terminate in the most weakly bound states at 280.2 meV.

$$\frac{dN(I)}{dt}=\sum_{J\neq I}[C(I,J)+A_r(I,J)+P(I,J)]N(J) \\ -N(I)\sum_{J\neq I}[C(J,I)+A_r(J,I)+P(J,I)]\ , \quad (28)$$

where I,J are particular ion configurations $(Z,\{i\})$, and where $C(I,J)N(J)$, $A_r(I,J)N(J)$, and $P(I,J)N(J)$ are the fluxes contributing to a decrease in $N(J)$ and an increase in $N(I)$ resulting from, respectively, collisional, radiative, and phonon processes. More specifically, (28) can be written for the ion configuration $X(Z-1,i)$ (for i in the conduction band) as

$$\frac{dN(Z-1,i)}{dt}=\sum_j N(Z-2,i,j)\left\{\sum_{f=c,v} n_f q_j^{fb}+\beta_{pi}(j)+A_{cv}(j)+\beta_{\mathrm{LO},i}(j)\right\} \\ +\sum_{j\neq i} N(Z-1,j)\sum_{f=c,v} n_f q_{ji}^{f}+\sum_{j>i} N(Z-1,j)[A_{ji}+B_{ji}\rho(\nu)]+\sum_{j<i} N(Z-1,j)B_{ji}\rho(\nu) \\ +N(Z)n_b\left\{\sum_{f=c,v} n_f\alpha_3^{fb}(i)+\alpha(i)+\beta_{rr}(i)+\alpha_{\mathrm{LO}}(i)+\beta_{\mathrm{LO},r}(i)\right\} \\ -N(Z-1,i)\left\{\sum_{f=c,v} n_f\left[q_i^{fb}+\sum_{j\neq i} q_{ij}^{f}\right]+\sum_{f=c,v} n_f n_b\sum_j \alpha_3^{fb}(j)\right. \\ +\sum_{j<i}[A_{ij}+B_{ij}\rho(\nu)]+\sum_{j>i} B_{ij}\rho(\nu)+n_b\sum_j\alpha(j)+n_b\sum_j\beta_{rr}(j)+\beta_{pi}(i)+A_{cv}(i) \\ \left.+n_b\sum_j\alpha_{\mathrm{LO}}(j)+n_b\sum_j\beta_{\mathrm{LO},r}(j)+\beta_{\mathrm{LO},i}(i)\right\}\ , \quad (29)$$

where we have included the contributions of adjacent ionization sequences to the fluxes resulting from collisional, radiative, and phonon processes.

Equations (29) are solved in the steady state subject to the boundary conditions that the total concentration of carriers in each band and the total concentration of ions are conserved. The total concentration of ions is found from the known spacing d (=400 Å in our example) between quantum-dot centers,

$$\sum_{\{I\}} N(\{I\})=\sum_{(Z,\{j\})} N(Z,\{j\})=N_{\mathrm{ion}}=d^{-3}\ . \quad (30)$$

The total concentration $n_{c,\mathrm{tot}}$ of conduction band electrons is

$$n_{c,\mathrm{tot}}=n_c+\sum_{\text{bound } i} n_i\ , \quad (31)$$

the sum of the concentration of the free electrons n_c and of the electrons in all bound states i. In (31), n_i is the number of electrons in the bound state i, averaged over all quantum-dot ion configurations,

$$n_i=\frac{\sum_{\{I\}} n_{i,I}N(\{I\})}{\sum_{\{I\}} N(\{I\})}\ , \quad (32)$$

where $n_{i,I}$ is the known number of electrons in the single particle state i in the particular quantum-dot ion configuration I.

As a check of our numerical rate equations, we have considered quantum dots which are doped with impurities to have the total electron concentration in (31) and no steady state hole population. These quantum dots are modeled to have no net interband radiative emission and no injected current. The steady state solution of the rate equations then gives an equilibrium distribution (26) of ion concentrations, as expected.

A. Solution of the rate equations for a particular example from the literature

To discuss the ionization balance in quantum dots, we solve the rate equations for a particular example[4] taken from the literature, that of 100-Å-radius GaAs quantum dots whose centers are separated by d=400 Å. The materials parameters for GaAs and the barrier material $Al_{0.3}Ga_{0.7}As$ barriers were given in the Introduction. Since typical bound *hole* states are separated by only a few[8] meV in our 100-Å-radius GaAs quantum dots, we will assume that the valence band is described by a quasiequilibrium (1). Thus, in this section, we are only interested in the rate equations describing the populations in quantum-dot *conduction* band states.

The total concentration of electrons and holes was chosen to be the same as that used in the example[4] from the literature, $n_{c,\mathrm{tot}}=3.125\times10^{16}$ cm^{-3}. This value of $n_{c,\mathrm{tot}}$ is equal to $2N_{\mathrm{ion}}=2d^{-3}$, corresponding to two electrons and two holes per quantum dot. Numerically, this means that there are three types of ion configurations to consider: nonionized (with Z=0 and two bound conduction band electrons per quantum dot), singly ionized (with Z=1 and one bound conduction band electron per quantum dot), and doubly ionized (with Z=2 and no bound conduction band electrons per quantum dot). Not including the angular momentum degeneracies in Table III, there are only ten types of single particle bound conduction band states to consider. (The angular momen-

tum degeneracies are accounted for by assuming that phonon scattering enables the occupation of degenerate states to be described by a quasiequilibrium distribution.) This problem is small enough for the concentrations of all the 66 types (1 doubly ionized, 10 singly ionized, and 55 nonionized) of ions to be found numerically.

The steady state ion population is found iteratively by guessing a value of the free electron concentration n_c and using a biconjugate gradient method to invert the matrix equation formed by (29) (with time derivatives set to zero) and (30). The ion population is used in (31), together with previous estimates of n_c, to get a quasi-Newton estimate of n_c.

Upon solution of the rate equations (29), the free electron concentration was found to be $n_c = 1.493 \times 10^{16}$ cm^{-3} and is a large fraction of the total concentration of conduction band electrons, $n_{c,\text{tot}} = 3.125 \times 10^{16}$ cm^{-3}. The concentration of doubly ionized quantum dots $N(Z=2)$ was found to be 4.356×10^{15} cm^{-3}, a large fraction of the total concentration of ions $N_{\text{ion}} = 1.5625 \times 10^{16}$ cm^{-3}. Table IV shows the concentrations of ions containing exactly one electron in a bound conduction band state. The concentrations of quantum dots with two bound conduction band electrons was found to be at least two orders of magnitude smaller than the typical concentrations shown in Table IV,[27] and are available from the author by request.

The deviation of the ionization balance from equilibrium is defined through the coefficients $b(Z=1,i)$ in

TABLE IV. The concentration of ions containing exactly one electron in a low lying conduction band bound state is much smaller than in quasiequilibrium (1) because interband spontaneous emission is much faster than capture rates into bound states from the continuum. Since the conduction band bound levels 8,9 are within a LO phonon energy of the barrier band edge at 289.1 meV, the concentrations $N(Z=1,8)$,$N(Z=1,9)$ are related to $N(Z=2)$, the concentration of quantum dots with no bound conduction band electrons, via a Saha-Boltzmann distribution, as indicated by a value of unity for $b(Z=1,8)$ and $b(Z=1,9)$ in (33). [$N(Z=1,i)$ is the concentration of those quantum dots whose one bound electron in state i.] $N(Z=2)$ was found from the rate equations to be 4.356×10^{15} cm^{-3}. The total concentration of ions is $N_{\text{ion}} = 1.5625 \times 10^{16}$ cm^{-3}, for quantum dots whose centers are separated by 400 Å. The concentrations of quantum dots with two bound conduction band electrons was found to be at least two orders of magnitude smaller than the typical concentrations shown in this table.

i	$N(Z=1,i)=N_i^+$ (10^{14} cm^{-3})
0	2.03
1	2.53
2	5.06
3	10.01
4	6.67
5	2.97
6	14.35
7	10.76
8	2.58
9	5.17

$$N(Z=1,i)=N(Z+1)\frac{g(Z,i)}{g(Z+1)}\frac{n_c}{N_C}\exp\left[\frac{U_i}{k_BT}\right]b(Z=1,i)\ , \tag{33}$$

where i is a bound state in the conduction band. For an ionization equilibrium, all the coefficients $b(Z=1,i)$ are equal to unity.

As a quick check of our numbers, observe that electrons in states connected by an acoustic or LO phonon are in LTE because the phonon absorption and emission rates (18) and (22) are much larger than all other transition rates. For example, Table IV shows that the ratio of the concentrations of ions having exactly one electron in bound state 2 to those with one in bound state 1 to be 2:1, which is exactly the ratio of their degeneracies (see Table III). As another example in Table IV, since the bound states 8,9 are within an LO phonon energy of the $Al_{0.3}Ga_{0.7}As$ band edge, then the concentrations $N(Z=1,8)$ and $N(Z=1,9)$ are related to the concentration of doubly ionized quantum dots $N(Z=2)$ through a Saha-Boltzmann equation (26) with a value of unity for $b(Z=1,8)$ and $b(Z=1,9)$. Equivalently, Fig. 6 shows both the electrons in the bound states 8,9 (located at 280.2 meV in the figure) and the free electrons to have the same quasiequilibrium ["Fermi-Dirac (free e's only)"] distribution whose Fermi level is determined by the *free* electron concentration 1.493×10^{16} cm^{-3} through $n_c/N_C \simeq \exp(E_{Fc}/k_BT)$.

Non-LTE occupation factors

By analogy with the occupation factor defined under the assumption of quasiequilibrium within an energy band (1), the quantum-dot conduction band bound state occupation factor is

$$f_c(E_i)=\frac{n_i}{g_i N_{\text{ion}}}\ , \tag{34}$$

where n_i is the number of electrons in the bound state i, averaged over all quantum-dot ion configurations (32).

Figure 6 shows the room-temperature quasiequilibrium distribution function (1) [Fermi-Dirac (all e's) with $E_{Fc} = 56.7$ meV corresponding to two electrons per quantum dot] commonly assumed in the literature for all conduction band electrons to be very different from our Rate Eqs (labeled as asterisks) solution (34). Equation (1) is assumed in work done at Caltech[4] for the conduction band of 100-Å-radius GaAs quantum dots whose centers are separated by 400 Å. Our rate equation solution is in good agreement with a simple model[28] of the random walk, as described by a Fokker-Planck equation in Sec. IV C, of electrons in energy. The small size of the Rate

Eqs occupation factors relative to the commonly assumed Fermi-Dirac (all e's) occupation factors is a result of the small size of the three-body recombination rates shown in Table III relative to interband spontaneous emission rates, as discussed in Sec. IV B. Clearly the quasiequilibrium assumption (1) is not valid for all conduction band electrons in our quantum-dot example.

B. Dominant processes determining the bound level occupations

As is the case in atomic plasmas, capture of free carriers via three-body recombination affects mainly high energy bound states located near the extended continuum, as indicated in Table III. Also by analogy with atomic plasmas, radiative recombination into bound states is important only when large ionization potentials are involved because of the cubic dependence of the Einstein A coefficient on radiative energy. Radiative recombination into the quantum-dot bound states in our example is shown to be insignificant (and three-body recombination to be significant) in Table III, and Figs. 7 and 8, because of the relatively large (1.493×10^{16} cm^{-3}) free carrier concentrations consistent with the current quantum-dot literature.

In this section, we show that collisional and interband radiative processes determine the quantum-dot ion and bound level populations. We will use Figs. 7 and 8 to show that after an electron is captured from the extended continuum into a weakly bound state, it drops into lower energy bound states mainly via collisional deexcitation until it combines with a valence band hole. For quantum dots, the extended continuum will usually include bound states within an LO phonon energy of the barrier band edge, as room-temperature LO phonon processes are much faster than all collisional and radiative processes.

Figures 7 and 8 show the relative contributions of various processes on the right hand side of (29) tending to decrease and increase, respectively, the concentration of singly ionized 100-Å-radius GaAs quantum dots at room temperature and a free electron concentration of $n_c=1.493\times10^{16}$ cm^{-3}. Contributions from quantum-dot ions having exactly two bound electrons were not considered in either of these two figures. Figure 7 shows that all singly ionized quantum dots, except those with an electron in bound states 8 or 9 at 280.2 meV, are depopulated mainly through collisional deexcitation or interband spontaneous emission. Figure 8 shows singly ionized quantum dots containing an electron in low energy bound states are populated mainly through collisional deexcitation. Singly ionized quantum dots containing an electron in an intermediate energy bound state are populated mainly through three-body recombination.

As shown in the figures, population and depopulation of the quantum-dot bound states by intraband radiative processes are much slower than by intraband collisional processes at this relatively large free carrier concentration because the typical adjacent bound state energy separations are relatively small (see Sec. III). Insignificant fluxes were found to result from processes which appeared in Tables II and III but which are not shown in Figs. 7 and 8.

In quantitative terms, one can use the numbers shown in Tables II–IV to show that [$N(Z=1,i)=N_i^+$ and $N(Z=2)=N^{+2}$]

$$n_c q_{41}^c N_4^+ \simeq [A_{cv}(1)+n_c q_{10}^c]N_1^+ , \tag{35}$$

$$n_c q_{74}^c N_7^+ \simeq n_c q_{41}^c N_4^+ , \tag{36}$$

$$n_c^2 \alpha_3^{cc}(7) N^{+2} \simeq [n_c q_{74}^c + n_c q_7^{cc} + A_{cv}(7)]N_7^+ . \tag{37}$$

These three equations show that after being captured into state 7, an electron [Eq. (37)] which does not ionize again and which does not combine with a valence band hole will collisionally deexcite [Eq. (37)] into bound state 4 from which it collisionally deexcites [Eq. (36)] into bound state 1.

The concentration N_1^+ is found from

$$[A_{cv}(1)+n_c q_{10}^c]N_1^+ \simeq \left[\frac{n_c q_{74}^c}{n_c q_{74}^c + n_c q_7^{cc} + A_{cv}(7)}\right] n_c^2 \alpha_3^{cc}(7) N^{+2} . \tag{38}$$

The fraction on the right-hand side above is the fraction of the electrons captured into bound state 7 which do not ionize (with rate q_7^{cc}) again and which do not combine with a valence band hole [with rate $A_{cv}(7)$]; it is about 0.5. The concentration N_1^+ is determined by the steady state flow via collisional deexcitation into level 1 resulting from this fraction of all electrons captured into state 7 by three-body recombination [$n_c^2\alpha_3^{cc}(7)=1/38.2$ ns] and the steady state flow out of level 1 through interband spontaneous emission [$A_{cv}(1)=1/9.4$ ns] and collisional deexcitation ($n_c q_{10}^c=1/23.3$ ns). N_1^+ is much smaller than N^{+2} because $n_c^2\alpha_3^{cc}(7)$ is much smaller than $A_{cv}(1)$. Similarly, one can show that

$$[A_{cv}(2)+n_c q_{20}^c]N_2^+ \simeq \left[\frac{n_c q_{63}^c}{n_c q_{63}^c + n_c q_6^{cc} + A_{cv}(6)}\right] n_c^2 \alpha_3^{cc}(6) N^{+2} . \tag{39}$$

C. Fokker-Planck equation of electron random walk in energy

The simple model presented in Sec. IV B shows that quantum-dot bound carriers relax to lower energy bound states via intraband collisional processes before combining with a valence band hole. Using ideas described[23,28] more fully in the atomic plasma literature, this collisional cascade can be modeled as the random walk of electrons through conduction band bound states via a Fokker-

Planck equation. Appendix E1 reviews Pitaevskii's[28] model of this electron collisional cascade as a "diffusion" in energy. In Appendix E2, we will follow Pert[23] in modifying Pitaevskii's[28] equations to include other processes (mainly interband radiative emission from and three-body recombination into conduction band bound states) involved in the relaxation of bound carriers to lower energies.

In this section, we highlight some of the results of Appendix E. Within reasonable assumptions, we will be able to calculate occupation factors analytically. We will find good agreement between our solution of the full rate equations and Appendix E.

From Appendix E2, the steady state downward flux in energy of bound carriers past the bound state with energy E is

$$-J=B(E)\left[\frac{dF}{dE}-\frac{F}{\rho}\frac{d\rho}{dE}+\frac{F}{k_BT}\right]+\int_E^{E_c}dE''F(E'')A_{cv}(E'')+\sum_{E''=E_{\min}}^{E}[n_c^2\alpha_3^{cc}(E'')N(Z+1)-n_cq_{E''}^{cc}N(Z,E'')]\ , \tag{40}$$

where the diffusion coefficient in the Fokker-Planck equation is

$$B(E_j)=\tfrac{1}{2}\sum_{E_{ji}}X(E_{ji})E_{ji}^2\ , \tag{41}$$

where $X(E_{ji})$ is the rate for the collisional process in which the bound particle makes a transition from state j to state i, where the energy density of states is $(\Delta E_j=E_{j+1/2}-E_{j-1/2})$

$$\rho(E_j)=g_j/\Delta E_j \tag{42}$$

and the distribution function in energy is

$$F(E_j)=N(Z,j)/\Delta E_j\ , \tag{43}$$

where $E_{\min}$ is the lowest energy conduction band bound energy, E_c is the energy above which a Saha-Boltzmann equilibrium exists with free electrons, and, in the notation of this paper, $A_{cv}(E)$ includes all rates originating at the conduction band bound energy E and terminating in the valence band,

$$A_{cv}(E'')=\int_{\text{valence band}}dE'F(E')A_{cv}(E'',E')\ , \tag{44}$$

where E'' is a conduction band and E' is a valence band bound energy. The assumption of a quasicontinuous distribution of states in (62) is valid whenever (60) can be approximated by (62). Numerically, we have verified this to be true for our quantum-dot example.

The first three terms in the parentheses in (40) is the downward flux resulting from collisional excitation and deexcitation only. [See Eq. (60).] The integral in (40) is the interband radiative flux originating from states with energy greater than E. The sum in (40) is the three-body recombination flux terminating in states with energy less than or equal to E.

Though Eq. (40) can be solved numerically for $N(Z,j)$, more insight would be obtained by making a few approximations. We will assume that the energy density of states $\rho(E')$ is roughly a constant, since the quantum-dot bound states shown in Table III have degeneracies which are constant to within a factor of 4 and since adjacent bound states are separated by roughly a constant amount (E_{ji} varies between 40 and 60 meV). We will also assume that $B(E)$ is roughly constant, since the collisional rates depend on the (roughly constant) intraband transition energy and initial degeneracies. (Table II shows the largest collisional rates all to be within the same order of magnitude.)

The discussion of Eqs. (E11) and (E12) in Appendix E shows that the quantum-dot bound level populations are determined mainly by the collisional cascade. Interband radiative emission and three-body recombination make smaller contributions, on the order of $\frac{1}{2}[2A_{cv}(E)(k_BT)^2/B(E)]\sim\frac{1}{8}$. As discussed in Appendix E, we can then make two further approximations: (i) that $A_{cv}(E)$ is relatively independent of the conduction band bound state energy E, and (ii) the net three-body recombination flux is largest for states near the barrier band edge.

Appendix E shows that when $[B(E)/2A_{cv}(E)(k_BT)^2]^{1/2}\sim 2$ or larger, which is true for our quantum dots, (40) yields the solution[29] for (33),

$$b(E)\simeq\exp[(E-E_c)/k_BT]\quad\text{for } E<E_c\ . \tag{45}$$

Since most of the electrons remain unbound, so that

$$N(Z=2)\sim N_{\text{ion}}\ , \tag{46}$$

the occupation factor for each of the single particle bound states E_i comes mainly from the singly ionized quantum dots and is approximately, using (33),

$$f_c(E_i)\simeq\frac{n_c}{N_C}\exp\left[\frac{U_i}{k_BT}\right]b(Z=1,i)\ . \tag{47}$$

Equations (45) and (47) yield

$$f_c(E_i)\simeq\frac{n_c}{N_C}\exp\left[\frac{V_B-E_c}{k_BT}\right]\quad E_i<E_c\ , \tag{48}$$

where V_B is the barrier band edge as measured from the quantum-dot band edge.

Equation (48) is plotted in Fig. 6 as the curve labeled "Fokker-Planck." In Fig. 6, we took E_c to be the barrier band edge V_B, above which a Saha-Boltzmann equilibrium exists with free electrons. Good agreement is observed between the results of our Rate Eqs and the Fokker-Planck solutions. This powerful result is an additional check of our simple model of the populating of quantum-dot bound levels via intraband collisional cascade of conduction band electrons followed by recom-

bination with a valence band hole.

The fact that the Rate Eqs. and Fokker-Planck solutions in Fig. 6 are (roughly) independent of bound state energy is a result of the roughly equal spacing between conduction band bound state energies, as the collisional rate coefficients are very similar for very similar intraband transition energies. The very similar values of collisional rate coefficients and intraband transition energies in our quantum dot, regardless of the initial bound energy, forces $B(E)$, and thus the occupation factor $f(E)$, to be roughly independent of bound state energy, as shown in Fig. 6 and Appendix E. This is a very important difference between atomic ions and quantum dots; the increasing bound energy separations for the lower energy bound states in atomic ions introduces the concept, not necessary for quantum dots, of a collisional limit, which separates the two regimes where collisions and radiative processes dominate.

V. CONCLUSIONS

We find the use of a quasiequilibrium particle distribution (1) with the same quasi-Fermi level E_F for all the quantum dot carriers in an energy (conduction or valence) band *not* to be valid for a wide range of temperatures (see Fig. 4) at the inversion populations and bound energy separations (greater than a LO phonon energy) assumed in the literature. An important consequence is that the Bernard-Duraffourg condition,[30] whose derivation assumes quasiequilibrium in each energy band, for net stimulated emission in conventional semiconductor lasers does not apply for quantum-dot semiconductor lasers. The condition for population inversion, as well as the calculation of the threshold current densities, in quantum dot lasers must account for the results of Sec. IV: both the non-LTE bound state populations and the large number of free carriers found in our example. This is the subject of a future work.

The bound state occupation factors in Fig. 6, obtained from the steady state solution of the rate equations (29) describing the ionization balance in the conduction band of room-temperature 100-Å-radius GaAs quantum dots whose centers are separated by 400 Å, are found to be very different from the commonly assumed quasiequilibrium distribution (1). Our numerical solution is in good agreement with Pitaevskii's model (Appendix E) from atomic physics of an electron random walk in energy, as modeled by a Fokker-Planck equation. Our simple model is that electrons captured into a quantum-dot conduction band bound state through three-body recombination and phonon emission drop into lower bound states through a series of collisional deexcitations before combining with a valence band hole.

Included in our rate equations are processes (Sec. II) which fundamentally exist even in ideal quantum dots for which trap and defect states have no significant effects: collisional excitation and deexcitation as well as collisional ionization[6] from and three-body recombination into all bound states resulting from the Coulomb interaction with incident free particles, interband spontaneous emission, intraband absorption and emission as well as photoionization and radiative recombination resulting from a Planck distribution of photons, ionization from and recombination into weakly bound states resulting from interaction with an equilibrium distribution of LO phonons, and excitation and deexcitation resulting from an equilibrium distribution of small energy acoustic phonons. The simple models for quantum-dot collisional rates presented in this paper are expected to be useful in giving convenient dependences on materials parameters, collisional exchange energies, and temperatures.

The critical free electron concentration (24) above which collisional processes can establish a quasiequilibrium, with its associated quasi-Fermi level E_{Fc}, in the conduction band is found to exceed 10^{19} cm^{-3} in our example.

ACKNOWLEDGMENTS

The author is greatly indebted to P. L. Hagelstein for many fruitful discussions and much encouragement. The AT&T Foundation and Rockwell International are gratefully acknowledged for financial support.

APPENDIX A: THE CLASSICAL PATH MODEL OF COLLISIONAL EXCITATION IN QUANTUM DOTS

We use the intermediate coupling strength form of the classical path (CP) method to describe collisional excitation in quantum dots. The suitability of this method for quantum dots has been discussed in detail[6] elsewhere. In this model, the collisional excitation cross section is

$$Q_{\mathrm{CPT}}(i\rightarrow j)=\left[\frac{m_i}{m_0}\right]\left[\frac{2\sum_{ij} f_{ji}}{3g_i}\right]\left[\frac{1}{E_{ji}E_{\mathrm{inc}}}\right]\left[\frac{e^2}{4\pi\epsilon_{ce}R}\right]^2[\phi(\beta_{\mathrm{co}})+\tfrac{1}{3}\zeta(\beta_{\mathrm{co}})](\pi R^2)\ , \tag{A1}$$

where m_i is the effective mass of the incident particle, R is the radius of the quantum dot, E_{inc} is the incident particle energy (measured from the band edge of the barrier material), f_{ji} is the oscillator strength obtained using (9) and summed over degenerate initial and final states, the appropriate dielectric constant is[6]

$$\epsilon_{ce}=\tfrac{1}{3}(\epsilon_{QD}+2\epsilon_{\mathrm{bar}}) \tag{A2}$$

(where $\epsilon_{QD},\epsilon_{\mathrm{bar}}$ are the quantum-dot and barrier dielectric constants) for collisions in which the incident particle does not penetrate the quantum dot, and β_{co} is the β parameter of Seaton,[31]

$$\beta_i=\frac{R_iE_{ji}}{\hbar v_{\mathrm{inc}}}=\left[\frac{2m_i}{\hbar^2}E_{\mathrm{inc}}\right]^{1/2}R_i\left[\frac{E_{ji}}{2E_{\mathrm{inc}}-E_{ji}}\right]\ , \tag{A3}$$

evaluated at the cutoff impact parameter R_{co}; the func-

tions $\phi(\beta_{co})$ and $\zeta(\beta_1)$ are given by Seaton.[31] The cutoff impact parameter R_{co} is chosen[32] to be the physical size of the target, which we define as the root mean square orbit size of the i,j states,

$$R_{co}=[\langle i|r^2|i\rangle\langle j|r^2|j\rangle]^{1/4} . \tag{A4}$$

In a previous[6] work, we have given another intermediate[32] form of the CP cross section, which accounts for the difference between the quantum dot and barrier dielectrics when the incident particle penetrates the quantum dot.

The collisional excitation rate coefficient is found by integrating the product of the free carrier velocity and (49) over a quasiequilibrium distribution of free carriers,

$$n_c q_{ji}^c \equiv n_c \langle v Q_{CPT}(i\rightarrow j)\rangle , \tag{A5}$$

of which more details have been given[6] in the literature.

Collisional rates in our example

A detailed discussion of the Van Regemorter and CP collisional excitation rates in quantum dots has been given[6] elsewhere. Collisional excitation and deexcitation rates for our 100-Å-radius GaAs quantum dots with a center-to-center separation of 400 Å are presented in Table II. The intraband oscillator strengths used are those calculated in Table I. The bound state energy levels and symmetries shown in Table III have been discussed[7,8,18] elsewhere. The free electron concentration was taken to be $n_c=1.493\times10^{16}$ cm^{-3} from the solution of the rate equations (29) (to be discussed in Sec. IV).

The collisional rates shown in Table II and in (A5) are usually largest for those states which have the smallest energy difference. For states separated by small energy differences, collisional deexcitation is much larger than intraband radiative emission.

B. THE BINARY ENCOUNTER MODEL OF COLLISIONAL IONIZATION IN QUANTUM DOTS

We use the binary encounter[33–36] model to describe collisional ionization in quantum dots, of which the suitability has been discussed in detail[6] elsewhere. The collisional ionization cross section in the symmetrized binary encounter (BE) model of Thomas and Burgess as described by Vriens[33,34] is

$$Q_i=\left[\frac{e^2}{4\pi\epsilon_{QD}}\right]^2\left[\frac{\pi}{E_1+U_i+E_2}\right]\left[\left[\frac{1}{U_i}-\frac{1}{E_1}\right]+\frac{2}{3}E_2\left[\frac{1}{U_i^2}-\frac{1}{E_1^2}\right]-\frac{1}{E_1+U_i}\ln\left|\frac{E_1}{U_i}\right|\right] , \tag{B1}$$

where $E_1\equiv\frac{1}{2}m^*v_1^2$ is the incident particle energy (measured from the quantum barrier band edge), $E_2\equiv\frac{1}{2}m^*v_2^2$ is the bound particle energy (measured from the quantum-dot band edge), and $U_i\equiv V_B-E_2$ is the ionization potential of (the bound) particle number 2. We have used the quantum-dot (and not the barrier) dielectric constant ϵ_{QD} as the relevant dielectric constant for the Coulomb interaction because this would be consistent[6] with the assumption of a near collision between the incident particle and the quantum dot.

The collisional ionization rate of an electron by an incident electron is, using (B1),

$$n_c q_i^{cc}\equiv n_c\langle Q_i v\rangle = n_c\left[\frac{e^2}{4\pi\epsilon_{QD}R}\right]^2\left[\frac{v_{th,C}R^2}{4\pi^{5/2}(k_BT)^2}\right]P_{BE}\left[\frac{U_i}{k_BT},\frac{E_2}{k_BT}\right] , \tag{B2}$$

where $P_{BE}(U_i/k_BT,E_2/k_BT)$ is an integral evaluated[6] in the literature.

Collisional rates in our example

A detailed discussion of collisional ionization out of a quantum-dot bound state has been given[6] elsewhere. Collisional ionization and three-body recombination rates for our 100-Å-radius GaAs quantum dots with a center-to-center separation of 400 Å are presented in Table III. The free electron concentration was taken to be $n_c=1.493\times10^{16}$ cm^{-3} from the solution of the rate equations (29).

In Sec. IV B, we construct a simple physical model (see Fig. 9) in which electrons are captured into a weakly bound state from continuum states (and states in LTE with the continuum) mainly through three-body recombination. We will see that the small size of the three-body recombination rates shown in Table III relative to interband spontaneous emission rates is the reason that most of the electrons in the conduction band remain free and are not in a quantum-dot bound state.

APPENDIX C: COMPARISON OF INTERBAND AND INTRABAND SPONTANEOUS EMISSION

We now show that interband spontaneous emission is usually stronger than intraband spontaneous emission. To show that interband spontaneous emission rates are almost always greater than intraband spontaneous emission rates, we first establish that the typical oscillator strengths associated with both interband and intraband transitions are comparable. This is done in Appendix D.

Having observed that the oscillator strength associated with both interband and intraband spontaneous emission are similar in magnitude, we note that interband transi-

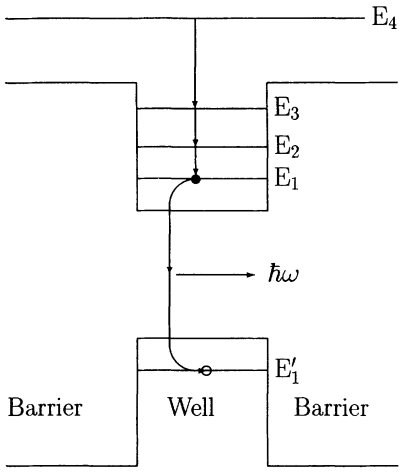

FIG. 9. Simple model for populating the conduction band bound states in our numerical example of 100-Å-radius GaAs quantum dots: after an electron is captured from the extended continuum (state 4 in the figure) into a weakly bound state (state 3 in the figure), it drops into lower energy bound states (states 1 and 2 in the figure) via collisional deexcitation until it combines with a valence band hole (state 1′ in the figure).

tions usually involve larger transition energies (greater than a bulk band gap energy) than intraband transitions. Of two processes with similar values of oscillator strengths, the one with the larger typical transition energies (interband spontaneous emission) would have the larger spontaneous emission rate, as indicated by (8). Thus, intraband spontaneous emission is too weak to establish a Saha-Boltzmann equilibrium within an energy band. In order for quasiequilibrium to be established within an energy band, we would require that the collisional excitation rates be at least comparable to interband spontaneous emission rates.

APPENDIX D: COMPARISON OF INTERBAND AND INTRABAND OSCILLATOR STRENGTHS

To show that interband spontaneous emission rates are almost always greater than intraband spontaneous emission rates, we first show that the typical oscillator strengths associated with both interband and intraband transitions are comparable. We now consider the interband oscillator strengths. We invoke the well known equation[37] for conduction band effective mass ($|j,\mathbf{k}=\mathbf{0}\rangle$ are bulk states at the Γ point),

$$\frac{m_0}{m_c}=1+\frac{2}{m_0}\sum_{j\neq i}\frac{|\langle i=CB,\mathbf{k}=\mathbf{0}|p_z|j,\mathbf{k}=\mathbf{0}\rangle|^2}{E_{i=CB,\mathbf{k}=\mathbf{0}}-E_{j,\mathbf{k}=\mathbf{0}}} \quad \text{(D1)}$$

and the definition[38] of oscillator strength, $f_{ji}\equiv(2m_0E_{ji}/\hbar^2)|\langle i|\mathbf{r}|j\rangle|^2=2|\langle i|p_z|j\rangle|^2/m_0E_{ji}$ to approximate the sum of the *inter*band oscillator strengths as

$$\sum_{i=VB} f_{i=VB,j=CB}\approx 1-\frac{m_0}{m_c} . \quad \text{(D2)}$$

Equation (D2) is only approximately true since it does not contain quantum-dot envelope overlap integrals, which are known[7] to deviate from unity.

Since the sum of the oscillator strengths is unity, we conclude that the sum of the *intraband* oscillator strengths is roughly

$$\sum_{i=CB} f_{i=CB,j=CB}\approx\frac{m_0}{m_c} . \quad \text{(D3)}$$

Equation (D3) can also be arrived at by approximating the quantum dot as having infinite potential barriers. By assuming that the conduction band is decoupled from the valence band, then the Hamiltonian inside the quantum dot in the effective mass approximation is $(\hbar^2/2m_c)\nabla^2$. For a free electron which has an effective mass m_c and which is governed by this Hamiltonian, the sum of the "effective" oscillator strengths is unity: $\sum_j(2m_cE_{ji}/\hbar^2)|\langle i|\mathbf{r}|j\rangle|^2=1$, for which (D3) becomes an equality. For small effective masses ($m_c=0.067$ for GaAs), (D2) and (D3) show that the typical interband and intraband oscillator strengths are comparable in magnitude.

APPENDIX E: FOKKER-PLANCK DESCRIPTION OF THE DIFFUSION IN ENERGY OF BOUND CARRIERS

The simple model presented in Sec. IV B shows that quantum-dot bound carriers relax to lower energy states by intraband collisional deexcitation before combining with a valence band hole. Using ideas from the atomic plasma literature,[23,28] this dominance of collisional processes in bound state transitions can be modeled as the random walk of electrons among bound states. In Appendix E1, we review the random walk of electrons through a set of discrete energy levels as modeled by Pitaevskii.[28]

In Sec. IV B, we found that interband radiative emission and three-body recombination, as well as collisional deexcitation, must be accounted for in determining the quantum-dot ion population. In Appendix E2, we will augment Pitaevskii's equations to include the downward flux in energy of conduction band bound carriers via interband radiative emission and three-body recombination. This will allow occupation factors to be calculated analytically within reasonable assumptions.

The steady state solution of the rate equations must satisfy

$$\sum_{j\neq 1}[X_{ji}N(Z,j)-X_{ij}N(Z,i)]=0 , \quad \text{(E1)}$$

where X_{ji} is the sum of the rates for all processes in which a carrier goes from state j to state i. It has the general solution[23,28]

$$\sum_{l=1}\sum_{i=0}\{X_{(j+l),(j-i)}N[Z,(j+l)] - X_{(j-i),(j+l)}N[Z,(j-i)]\}=-J , \quad \text{(E2)}$$

where $-J$ is the downward flux of carriers past state $(j+\frac{1}{2})$.

1. Intraband collisional processes only

When only terms with small l and i contribute significantly in (E2), and when X_{ij} and X_{ji} are related by detailed balance,

$$X_{ji}=\frac{g_i}{g_j}X_{ij}\exp\left[\frac{E_{ji}}{k_BT}\right], \tag{E3}$$

then Eq. (E2) can be written as a Fokker-Planck equation[23,28] for a steady state problem,

$$-J=B(E)\left[\frac{dF}{dE}-\frac{F}{\rho}\frac{d\rho}{dE}+\frac{F}{k_BT}\right]. \tag{E4}$$

If we impose the boundary conditions[23,28] that the bound carriers with energy greater than or equal to E_c (near the barrier band edge) are in Saha-Boltzmann equilibrium with free carriers, and that bound states very far below the barrier band edge ($E_j\rightarrow E_{\min}$) have zero occupation [$F(E_j\rightarrow E_{\min})=0$],[39] then the solution to (E4) is[23,28]

$$F(E)=\frac{n_c}{N_C}\frac{N(Z+1)}{g(Z+1)}\rho(E)\exp[(E_c-E)/k_BT]b(E) \tag{E5}$$

with the deviation from Saha-Boltzmann equilibrium given by

$$b(E)=\frac{\int_{E_{\min}}^{E}dE'\dfrac{\exp[(E'-E_c)/k_BT]}{\rho(E')B(E')}}{\int_{E_{\min}}^{E_c}dE'\dfrac{\exp[(E'-E_c)/k_BT]}{\rho(E')B(E')}}\quad\text{for } E<E_c\ . \tag{E6}$$

The bound carriers with energy greater than or equal to E_c are in Saha-Boltzmann equilibrium with free carriers,

$$b(E)=1\quad\text{for } E>E_c\ . \tag{E7}$$

As discussed in Sec. IV C, we can approximate $\rho(E')$ and $B(E)$ as constant in E, and (E6) reduces to

$$b(E)=\begin{cases}\exp[(E-E_c)/k_BT] & \text{for } E<E_c\\ 1 & \text{for } E>E_c\ .\end{cases} \tag{E8}$$

Equation (E8) shows that the deviation from a Saha-Boltzmann equilibrium is greatest for states very far from the continuum.

2. Inclusion of capture and interband radiative processes

When three-body capture and interband radiative processes are included, the steady state downward flux past the bound state with energy E is

$$-J=B(E)\left[\frac{dF}{dE}-\frac{F}{\rho}\frac{d\rho}{dE}+\frac{F}{k_BT}\right]+\int_E^{E_c}dE''F(E'')A_{cv}(E'')+\sum_{E''=E_{\min}}^{E}[n_c^2\alpha_3^{cc}(E'')N(Z+1)-n_cq_{E''}^{cc}N(Z,E'')]\ , \tag{E9}$$

where $E_{\min}$ is the lowest energy conduction band bound energy.

Though (E9) can be solved numerically, a few approximations allow a simple analytical answer which provides physical insight. Clearly, if the sum of the fluxes resulting from the net three-body capture and the interband radiative processes [the sum and the integral in (E9)] is a constant, then (E6) still applies. Thus, Eq. (E6) applies whenever the flux resulting from the net collisional deexcitation is constant.

For our quantum-dot example, we find that we can make the numerical approximation

$$\int_E^{E_c}dE''F(E'')A_{cv}(E'')+\sum_{E''=E_{\min}}^{E}[n_c^2\alpha_3^{cc}(E'')N(Z+1)-n_cq_{E''}^{cc}N(Z,E'')]\simeq[E_c-E]F(E)A_{cv}(E)\ , \tag{E10}$$

which, with (E9), says that the downward flux resulting from collisional processes is linear in the bound state energy to within an additive constant.

The right hand side of (E10) comes from two approximations: (i) that $A_{cv}(E)$ is relatively independent of the conduction band bound state energy E, and (ii) the net three-body recombination flux is largest for states near the barrier band edge. Approximation (ii) allows us to ignore the net three-body recombination in comparison with interband radiative rates on the right hand side of (E10). Departure from the approximation (i) comes from the hole population function $F(E)$ in (44); $A_{cv}(E)$ would be independent of E if the same population $F(E)$ existed for all holes with a wave vector matching a conduction band bound state wave vector (in a model in which light and heavy hole states were[7,8,18] decoupled). Table III shows $A_{cv}(E)$ to remain constant to within a factor of 5 for the states shown. Approximation (ii) is almost always true because of the decaying exponential dependence of the collisional ionization[6] rates on the ionization potential.

With the approximation (E10) and constant values of $\rho(E)$ and $B(E)$, one can show that the deviation from Saha-Boltzmann equilibrium is

$$b(E)=\exp\left[\frac{A_{cv}(E)}{2B(E)}[E-E_c]^2\right]\operatorname{erfc}\left[\sqrt{A_{cv}(E)/2B(E)}\left[E_c-E+\frac{B(E)}{A_{cv}(E)k_BT}\right]\right]$$
$$\times\left\{\operatorname{erfc}\left[\sqrt{A_{cv}(E)/2B(E)}\left[\frac{B(E)}{A_{cv}(E)k_BT}\right]\right]\right\}^{-1} \quad \text{for } E<E_c \ . \tag{E11}$$

When $[B(E)/2A_{cv}(E)(k_BT)^2]^{1/2}\sim 2$ or larger, (69) reduces to

$$b(E)\simeq\exp[(E-E_c)/k_BT] \quad \text{for } E<E_c \ , \tag{E12}$$

which agrees with (E8) and makes sense, as this is the limit in which interband radiative rates do not have a large effect on the collisional random walk. For our quantum dots, (E12) is applicable, and (47) becomes

$$f_c(E_i)\simeq\frac{n_c}{N_c}\exp\left[\frac{V_B-E_c}{k_BT}\right] \quad \text{for } E_i<E_c \ , \tag{E13}$$

where V_B is the barrier band edge as measured from the quantum-dot band edge. In Fig. 6, we took E_c to be the barrier band edge V_B, above which a Saha-Boltzmann equilibrium exists with free electrons.

*Mailing address: 350 Memorial Drive, Cambridge, MA 02139-4304.

[1]M. Asada, Y. Miyamoto, and Y. Suematsu, IEEE J. Quantum Electron. **QE-22**, 1915 (1986).
[2]Y. Arakawa and H. Sakai, Appl. Phys. Lett. **40**, 939 (1982).
[3]Y. Miyamoto, Y. Miyake, M. Asada, and Y. Suematsu, IEEE J. Quantum Electron. **QE-25**, 2001 (1989).
[4]K. J. Vahala, IEEE J. Quantum Electron. **QE-24**, 523 (1988).
[5]H. Sakaki, Jpn. J. Appl. Phys. **28**, L314 (1989).
[6]J. L. Pani, Phys. Rev. B **49**, 2554 (1993).
[7]J.-B. Xia, Phys. Rev. B **40**, 8500 (1989).
[8]J. L. Pan, Phys. Rev. B **46**, 4009 (1992).
[9]J. L. Pan (unpublished).
[10]G. P. Agrawal and N. K. Dutta, *Long Wavelength Semiconductor Lasers* (Van Nostrand Reinhold, New York, 1986).
[11]B. K. Ridley, *Quantum Processes in Semiconductors* (Oxford University Press, New York, 1988).
[12]A. Yariv, *Quantum Electronics* (Wiley, New York, 1975).
[13]*Handbook of Chemistry and Physics,* edited by R. C. Weast (CRC Press Inc., Boca Raton, FL, 1989).
[14]*Numerical Data and Functional Relationships in Science and Technology,* Landolt-Börnstein, New Series, Vol. 17, Pt. b (Springer-Verlag, New York, 1982).
[15]R. W. P. McWhirter, Phys. Rep. **37**, 165 (1978).
[16]A. Burgess and H. P. Summers, Mon. Not. R. Astron. Soc. **174**, 345 (1976).
[17]The principle of detailed balance, as in (3) and (5), arises from the fact that each term in the sum in a quasiequilibrium partition function must differ from every other term by a Boltzmann factor. The derivative of this partition function with respect to the quasiequilibrium fugacity gives the quasiequilibrium occupation factors in (1), where we have assumed that $n_c/N_C\simeq\exp(E_{Fc}/k_BT)$ with E_{Fc} measured from the barrier band edge.
[18]P. C. Sercel and K. J. Vahala, Phys. Rev. B **42**, 3690 (1990).
[19]E. O. Kane, J. Phys. Chem. Solids **1**, 249 (1957).
[20]J. L. Pan, Phys. Rev. B **46**, 3977 (1992).
[21]J. L. Pan (unpublished).
[22]M. C. Klein, F. Hache, D. Ricard, and C. Flytzanis, Phys. Rev. B **42**, 11 123 (1990).
[23]G. J. Pert, J. Phys. B **23**, 619 (1990).
[24]As discussed in Sec. IV, the holes in our quantum-dot example have a quasi-equilibrium distribution.
[25]If all quantum dot ion concentrations satisfy (26), then the partition function gives the occupation factors in (1), where we have assumed that $\exp(E_{Fc}/k_BT)\simeq n_c/N_C$ with E_{Fc} measured from the barrier band edge.
[26]R. W. P. McWhirter, in *A Survey of Phenomena in Ionized Gases,* Invited Papers at the Eighth International Conference on Phenomena in Ionized Gases (International Atomic Energy Agency, Vienna, 1968).
[27]The bound energy levels shown in Table III were found in the approximation that the GaAs quantum dot is surrounded by infinitely high potential barriers. Thus, the bound states closest to the $Al_{0.3}Ga_{0.7}As$ band edge at 289.1 meV will be the least accurately described by this model. However, the populations of these states are known; as discussed in Sec. IV B, the electrons in these bound states near the $Al_{0.3}Ga_{0.7}As$ band edge are expected to be in equilibrium with the free electrons because these bound states are within a LO phonon energy of the $Al_{0.3}Ga_{0.7}As$ band edge. Thus, the population distribution in the lower energy bound states is what is of interest to us, and these lower energy bound states can be described within the approximation of infinite potential barriers surrounding the GaAs quantum dot.
[28]L. P. Pitaevskii, Sov. Phys. JETP **15**, 919 (1962).
[29]Equation (45) is valid under the assumptions made so far, as long as there is a single dominant process (collisional, radiative, or phononic) affecting the random walk in (41).
[30]M. G. A. Bernard and G. Duraffourg, Phys. Status Solidi **1**, 699 (1961).
[31]M. J. Seaton, Proc. Phys. Soc. **79**, 1105 (1962).
[32]P. L. Hagelstein (unpublished).
[33]L. Vriens, in *Case Studies in Atomic Collision Physics I,* edited by E. W. McDaniel and M. R. C. McDowell (Wiley, New York, 1969), p. 335.
[34]L. Vriens, Proc. Phys. Soc. **89**, 13 (1966).
[35]M. R. C. McDowell, Proc. Phys. Soc. **89**, 23 (1966).
[36]J. S. Hansen, Phys. Rev. A **8**, 822 (1973).
[37]W. A. Harrison, *Solid State Theory* (Dover, New York, 1980).
[38]E. Merzbacher, *Quantum Mechanics* (Wiley, New York, 1970).
[39]The Fokker-Planck equation with this boundary condition is valid (Refs. 23 and 28) when $E_{\min}$ is far enough away [in terms of the transition lifetime X_{ji} in (60)] from the energy continuum.